Research Article

Yaning Zhou, Haizi Yao, Chundong Liu, Mengyu Chen, Chao Zhang, Mei Liu, Jian Wang, Fujun Zhang*, Jing Yu*, Baoyuan Man and Qianqian Sun*

High-performance flexible surface-enhanced Raman scattering substrate based on the particle-in-multiscale 3D structure

https://doi.org/10.1515/nanoph-2021-0381
Received July 15, 2021; accepted September 19, 2021;
published online September 30, 2021

Abstract: Recently, multiscale three-dimensional (3D) structures consisting of micrometer-scale structure and nanometer-scale structure have received some attention from scientists in the field of surface-enhanced Raman scattering (SERS). In this work, micrometer-scale grating structure and nanometer-scale zinc oxide nano spikes (ZnO NSs) structure are successfully introduced into the SERS substrate with silver nanoparticles (Ag NPs) as the surface plasmon. The optimized particle-in-multiscale 3D substrate (PDMS/grating/ZnO NSs/Ag NPs) presents high sensitivity with an ultralow limit of detection of 1×10^{-11} M and a high enhancement factor of 7.0×10^{8} for Rhodamine 6G (R6G) as the probe molecule. It benefits from the electromagnetic field enhancement from the excellent optical capture capability of grating/ZnO NSs structure and abundant electromagnetic hot spots. The quantitative analysis ability of the SERS substrate can be indicated from the good linear correlation between the logarithmic Raman intensity and the molecular concentration. At the same time, this SERS substrate exhibits excellent homogeneity and reproducibility, which have low relative standard deviations (4.43%) of the Raman intensities at 613 cm^{-1} peaks for R6G as the probe molecule. In addition, this SERS substrate can realize *in-situ* detection of Raman signal due to its excellent light transmission and flexibility. The particle-in-multiscale 3D structure as SERS substrate exhibits the vast potential in practical applicability for qualitatively and quantitatively chemical and biomedical analysis.

Keywords: grating; multiscale 3D structure; surface-enhanced Raman scattering; ZnO nanospikes.

1 Introduction

Surface-enhanced Raman scattering (SERS) has been regarded as one of the most powerful analytical tools for detecting molecules. SERS as a nondestructive spectroscopy technique plays a vital role in food safety, medical diagnostics, and environmental monitoring [1–3]. Precious metals nanostructures are widely used in SERS substrate due to their strong localized surface plasmon resonance (LSPR) effect in the hot spots that exist at the nanogaps between two metal nanoparticles (NPs) or the apex of metal tips. However, poor uniformity and reproducibility of precious metal matrix restricted its development in the practical application of SERS substrate. To achieve average ultrasensitive detection on the large area, three-dimensional (3D) nanostructures have been widely introduced to the SERS substrate to achieve more accessible and homogeneous hot spots [4–6]. The particle in 3D structure component of precious metal NPs and micro-nano structure shows great advantage in precise control localized electromagnetic fields [7–10]. Compared with particles in conventional two-dimensional structures, optical field mode around metal NPs of particles in 3D structures can be effectively amplified due to the periodic or quasi-periodic micro-nano structures. In the meantime, the

Yaning Zhou and Haizi Yao contributed equally to the work.

***Corresponding authors: Jing Yu and Qianqian Sun**, Collaborative Innovation Center of Light Manipulations and Applications in Universities of Shandong, School of Physics and Electronics, Shandong Normal University, Jinan 250014, China, E-mail: yujing1608@sdnu.edu.cn (J. Yu), qianqiansun@sdnu.edu.cn (Q. Q. Sun). https://orcid.org/0000-0003-2289-0748 (J. Yu), https://orcid.org/0000-0002-6204-168X (Q. Q. Sun); and **Fujun Zhang**, Key Laboratory of Luminescence and Optical Information, Ministry of Education, Beijing Jiaotong University, Beijing 100044, China, E-mail: fjzhang@bjtu.edu.cn
Yaning Zhou, Chundong Liu, Mengyu Chen, Chao Zhang, Mei Liu and Baoyuan Man, Collaborative Innovation Center of Light Manipulations and Applications in Universities of Shandong, School of Physics and Electronics, Shandong Normal University, Jinan 250014, China. https://orcid.org/0000-0002-3295-8980 (C. Zhang)
Haizi Yao, Key Laboratory of Smart Lighting in Henan Province, School of Energy Engineering, Huanghuai University, Zhumadian 463000, China
Jian Wang, College of Physics and Electronic Engineering, Taishan University, Taian 271021, China

particles in 3D structures are beneficial for the enrichment of probe molecules around metal NPs, which are also suitable for the Raman detection of low concentration probe molecules. More importantly, the high-density and homogeneous spatial hot spots can be formed for the particles in 3D structures to enlarge the electromagnetic field area, which can be modulated within the 3D structure with the zone ranging from several nanometers to hundreds of nanometers. The amplified optical field, the enriched probe molecules, and enlarge electromagnetic field area of particles in 3D structure can provide more significant and comprehensive electromagnetic enhancement. The more and more particles in 3D structures by integrating the NPs with the surrounding periodic or quasi-periodic micro-nano structures were demonstrated as efficient SERS substrates to enhance the SERS performance. The periodic or quasi-periodic micro-nano structures can come from the natural organism or artificial synthesis. Naturally quasi-periodic micro-nano structures can be obtained from the natural organism, such as rose petals, taro leaves, diatoms, and cicada wings [11–13]. Unnatural periodic or quasi-periodic micro-nano structures can be derived from the growing of metal, metal oxide, or organic compounds by different grown methods, such as grating, pyramid, bowl-shaped cavity, nanowires (NWs), nanosheets, nanotaper, nanorod, nanopore, NP, nanoring, and nanotube arrays [14–17].

Recently, the multiscale 3D structures consisting of micrometer-scale structure and nanometer-scale structure have received some attention from scientists in the field of SERS. A novel SERS substrate with regular silicon (Si) micro pyramids with the height of 940 nm and regular silver (Ag) nano bowls (the height of 180 nm, wall thickness of 100 nm) was designed by Jin et al., which have excellent capability of trapping light playing a significant role in the enhancement of Raman signal [18]. Zhao et al. demonstrated that the Au nanoparticles (Au NPs) in pyramid Si (PSi) (the 3 μm average height, the 4 μm average space)/molybdenum disulfide (MoS_2) (the average 12 nm wall thickness, the average 150 nm length, and the average 100 nm pore caliber) can serve as highly sensitive, uniform, and stable SERS substrates, which benefits from the synergistic effect of the enhanced light trapping of micrometer-scale PSi and nanometer MoS_2 and the effective plasmon couple [19]. Xu et al. demonstrated that the Ag NPs in the multiscale structure of pyramidal PDMS ($1.5 \times 1.5 \times 1\ \mu m^3$)/CuO NWs with tens of nanometers in diameters can be used as a highly sensitive SERS substrate with a micrometer-scale pyramidal structure for light confinement and nanometer-scale NWs for molecular enriching [20]. Compared with the normal metal in 3D structure, the metal-in-multiscale 3D structure component of metal films or NPs in multiscale structure can further effectively improve the propagation path of light, and more precisely control the localized electromagnetic fields.

In this work, the multiscale 3D structure of micrometer-scale grating structure and nanometer-scale Zinc oxide nano spikes (ZnO NSs) structure were successfully introduced into the SERS substrate with Ag NPs as the surface plasmon. The transparent and flexible PDMS substrates with the grating structure are obtained by copying the grating structure on the polycarbonate (PC) layers of the compact disc (CD-R). The ZnO NSs were synthesized on PDMS/grating substrates by the hydrothermal method [21]. Finally, Ag NPs were prepared on the surface of PDMS/grating/ZnO NSs substrates by thermal evaporation. The detailed experimental information is shown in the experimental section of the supporting information. The schematic diagram of the fabrication process of particle-in-multiscale 3D structure (PDMS/grating/ZnO NSs/Ag NPs) is shown in Figure 1. Compared with the PDMS/grating/Ag NPs SERS substrates or PDMS/ZnO NSs/Ag NPs SERS substrates, the particle-in-multiscale 3D structure has the highest sensitivity with an ultralow limit of detection (LOD) of 1×10^{-11} M and a high enhancement factor (EF) of 7.0×10^8 for Rhodamine 6G (R6G) as the probe molecule. It benefits from the electromagnetic field enhancement from the more and stronger hot spots from Ag NPs in ZnO NSs surface and the excellent optical capture capability of grating/ZnO NSs multiscale structure. At the same time, this SERS substrate exhibits excellent homogeneity and reproducibility, which has low relative standard deviations (RSD) (4.43%) of the Raman intensities at 613 cm^{-1} peaks for R6G as the probe molecule. In addition, the particle-in-multiscale 3D structure as SERS substrates can realize *in-situ* detection of Raman signal due to its excellent light transmission and flexibility, which has exhibited vast potential in practical applicability.

2 Results and discussions

The morphologies of PDMS/grating, PDMS/grating/ZnO NSs, and PDMS/grating/ZnO NSs/Ag NPs substrates were measured by scanning electron microscopy (SEM). The transparent and flexible PDMS substrates with the grating structure were obtained by copying the grating structure on the PC layers of CD-R. The grating structure on the surface of PDMS is complementary to that of PC layers, as shown in Figure S1. The period, the groove width and groove depth of grating on the surface of PDMS are about 1500, 1000, and 170 nm, as shown in Figure 2a. The SEM morphology image with a low magnification of PDMS/grating/ZnO NSs is shown in Figure 2b. When PDMS with the grating structure

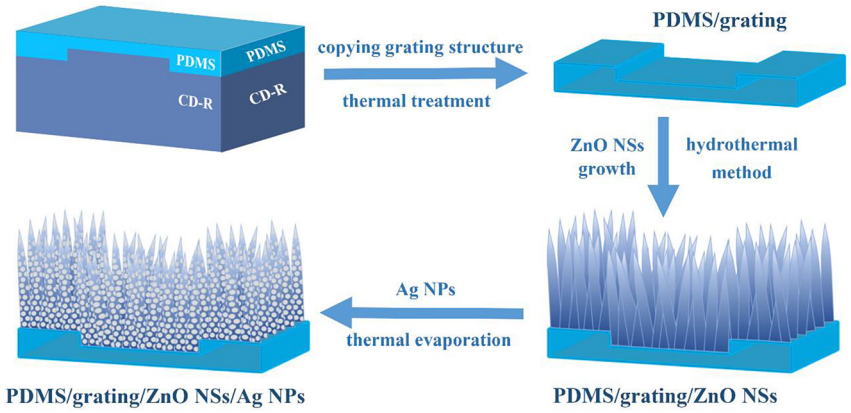

Figure 1: Schematic diagram of the fabrication process of particle-in-multiscale 3D substrate (PDMS)/grating/zinc oxide nano spikes (ZnO NSs)/silver nanoparticles (Ag NPs) substrates.

is covered with a large number of ZnO NSs by the hydrothermal method (as shown in Figure S2), the grating structure can still be seen clearly. This indicates that the periodic grating structure was formed on the surface of the ZnO NSs array, which ensures the coexistence of the micrometer-scale grating structure and the nanometer-scale nano spikes structure. To get a better look at the distribution of the ZnO NSs arrays, the top view and side view SEM images with larger magnification were measured and are shown in Figure 2c–d. The ZnO NSs are thicker at the bottom and thinner at the top, and they are evenly distributed over the grating structure. The average height of the ZnO NSs is about 462 nm as shown in Figure 2g. The average waist diameter between the ZnO NSs is 57 nm as shown in Figure 2h. Most of the angle is less than 30° between the growth direction of ZnO NSs and the normal direction of the substrate. The cross-contact between the ZnO NSs is possible due to the inclined angle of ZnO. Ag with different deposition thicknesses was deposited on the PDMS/grating/ZnO NSs substrate by thermal evaporation. The deposition thicknesses of Ag were adjusted from 4 to 16 nm with a 3 nm increment.

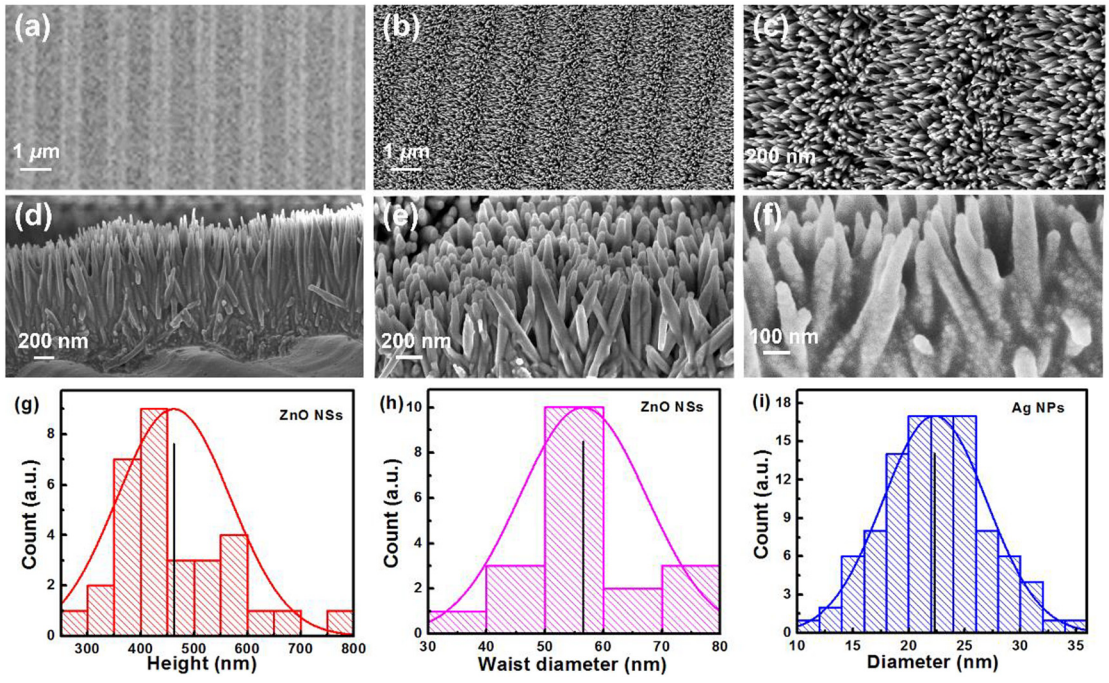

Figure 2: Top view scanning electron microscopy (SEM) images of the particle-in-multiscale 3D substrate (PDMS)/grating substrate (a) and PDMS/grating/zinc oxide nano spikes (ZnO NSs) substrate (b–c). Side view SEM images of PDMS/grating/ZnO NSs substrate (d) and PDMS/grating/ZnO NSs/Ag NPs substrate (e–f). Statistical value for the height of the ZnO NSs (g), the waist diameter between the ZnO NSs (h), and the diameter of silver nanoparticles (Ag NPs) (i).

A series of Raman spectra with R6G as the probe molecule was tested to quantitatively evaluate the Raman enhancement ability of the PDMS/grating/ZnO NSs/Ag as substrates. The excitation source is a 532 nm laser for the SERS measurements. All Raman spectra were collected under the same conditions, as shown in the experimental section of supporting information. The Raman characteristic peaks (613, 774, 1185, 1315, 1365, 1508, and 1650 cm^{-1}) of R6G with a concentration of 10^{-6} M can be observed in all the Raman spectra for PDMS/grating/ZnO NSs/Ag substrates with different Ag deposition thickness, as shown in Figure 3a. The corresponding vibrational modes of characteristic peaks are shown in Table S1. The corresponding Raman intensities of the peaks at 613, 774, and 1650 cm^{-1} dependence on the deposition thickness of Ag are described in Figure 3b. The relative intensities of the peaks at 613, 774, and 1650 cm^{-1} exhibit a similar trend, which is increases and then decreases with the increase of Ag deposition thickness. The highest SERS intensity of R6G with a concentration of 10^{-6} M has been obtained from the PDMS/grating/ZnO NSs/Ag NPs substrates with 10 nm deposition thickness of Ag. The side view SEM images of PDMS/grating/ZnO NSs/Ag NPs (10 nm deposition thickness of Ag) substrate were measured and are shown in Figure 2e, f. When Ag with 10 nm deposition thickness was deposited on the PDMS/grating/ZnO NSs substrate, the Ag NPs were uniformly deposited on the surface of ZnO NSs. The structures of nano spikes and grating still exist, which have not been overlaid. The average diameter of the Ag NPs is about 22 nm and the average gap of the Ag NPs is about several nm, as shown in Figure 2f and i. This means that the SERS intensities are closely related to the size, and gap of plasmon NPs, and there is an optimum value for size as well as gap [22–24].

The Raman spectra of R6G with a concentration varying from 10^{-5}~10^{-12} M on the PDMS/grating/ZnO NSs/Ag NPs (10 nm deposition thickness of Ag) substrate were detected and are shown in Figure 4a to evaluate the performance of the particle-in-multiscale 3D structure as SERS substrates. The intensities of the SERS signal are gradually enhanced with the increase of the R6G molecular concentrations. When the concentrations of R6G are 10^{-12} M, the SERS signal of R6G can be only obtained from the edge of the final evaporation imprint. Thus, to guarantee the scientific nature of the results, the 10^{-11} M was chosen as the LOD of the R6G solution for the calculation of the EF. The EF of PDMS/grating/ZnO NSs/Ag NPs substrates were calculated according to the standard equation:

$$\mathrm{EF} = \frac{I_{SERS}/N_{SERS}}{I_{RS}/N_{RS}}$$

where I_{SERS} and I_{RS} are the intensity of the SERS intensity obtained from the PDMS/grating/ZnO NSs/Ag NPs substrate and the normal Raman scattering intensity obtained from the flat PDMS substrate under identical test conditions, respectively. N_{SERS} and N_{RS} represent the number of probe molecules within the laser spot for SERS and normal Raman intensities on the PDMS/grating/ZnO NSs/Ag NPs substrate and the flat PDMS substrate, respectively. The value of N_{RS}/N_{SERS} was estimated from the ratio of the average areal density (AD) of the R6G on the flat PDMS substrate and the PDMS/grating/ZnO NSs/Ag NPs substrate due to the same laser spot of 1 μm. The calculation method of the average AD is shown in the supporting information. The relative Raman intensity of the 613 cm^{-1} peak of R6G with a lower concentration of 10^{-11} M is ~54 for PDMS/grating/ZnO NSs/Ag NPs substrates. The background spectrum of the substrate without probe molecule has been plotted underneath the lowest concentration spectrum for comparison, as shown in Figure S3. The noise threshold and the standard deviation of the background signal are 25 and 5.2%, respectively. The relative Raman intensity of ~54 for the 613 cm^{-1} peak of R6G with a lower concentration of 10^{-11} M is 2.2 times the noise threshold. It means that the 10^{-11} M R6G solution can be chosen as the LOD. The flat PDMS substrate is selected as the reference substrate. I_{RS} of 193 is obtained from the Raman spectrum of R6G with a higher concentration of 10^{-2} M collected on flat PDMS substrate, as shown in Figure S4. The AD of the R6G with the concentration of 10^{-2} M on the flat PDMS

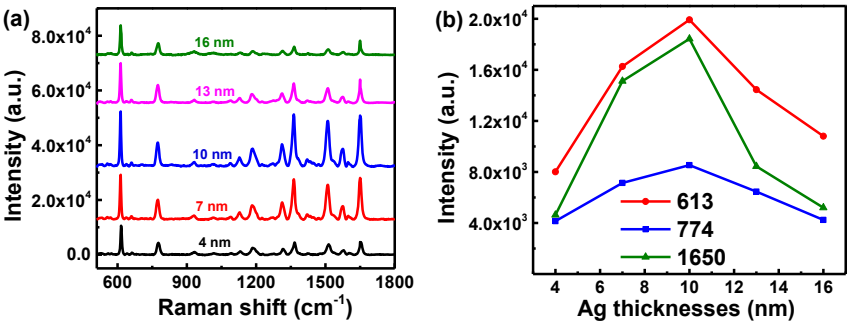

Figure 3: (a) Raman spectra of R6G with a concentration of 10^{-6} M on the particle-in-multiscale 3D substrate (PDMS)/grating/zinc oxide nano spikes (ZnO NSs)/silver nanoparticles (Ag NPs) substrates with different deposition thicknesses of Ag. (b) Corresponding Raman intensity of the peaks at 613, 774, and 1650 cm^{-1}.

substrate is around 6.0×10^9 molecules/μm^2. The AD of the R6G with the concentration of 10^{-2} M on the fabricated PDMS/grating/ZnO NSs/Ag NPs substrate is around 2.4 molecules/μm^2. The calculated EF of PDMS/grating/ZnO NSs/Ag NPs substrate is 7.0×10^8 according to the $I_{SERS}/I_{RS} \approx 0.28$, $N_{RS}/N_{SERS} \approx 2.5 \times 10^9$. To illustrate the sensitivity of PDMS/grating/ZnO NSs/Ag NPs as SERS substrates, some representative works with the particle in ZnO structure, particle in grating structure, and particle-in-MSC 3D structure as SERS substrate are shown in Table S2. The contrast data of EF and LOD for different SERS substrates can show that the PDMS/grating/ZnO NSs/Ag NPs as SERS substrates have high sensitivity [25–27].

The relationship between Raman intensities of 613 cm^{-1} peaks and the logarithm of the concentrations of R6G (10^{-5}~10^{-12} M) was fitted by the Langmuir isotherm model, as shown in Figure S5 [28–30]. The high determination coefficients (R^2) are 0.997 for 613 cm^{-1} peaks for Langmuir isotherm fitting. This means that the actual Raman intensities for the wide range of concentrations are suitable for nonlinear Langmuir isotherm fitting. To investigate the ability of quantitative detection, the functional relationship between the Raman intensity of R6G at 613 and 774 cm^{-1} peaks with the R6G molecular concentrations (10^{-6}–10^{-11} M) are fitted and are shown in Figure 4b and Figure S6. The fitting formulas are LogI = 0.54LogC+7.62 and LogI = 0.52LogC+7.15 for 613 and 774 cm^{-1}, where I and C represent the intensity of R6G and the concentration of R6G. The high R^2 are 0.987 and 0.993 for 613 and 774 cm^{-1} peaks, respectively. It indicates the Raman intensities have a good linear relationship with different R6G concentrations. Except for sensitivity, the homogeneity and reproducibility of the SERS substrates play important parts in practical applications as well. The twenty Raman spectra of R6G with a concentration of 10^{-6} M on the PDMS/grating/ZnO NSs/Ag NPs substrates were randomly collected from different 20 batches, as shown in Figure 4c. The Raman

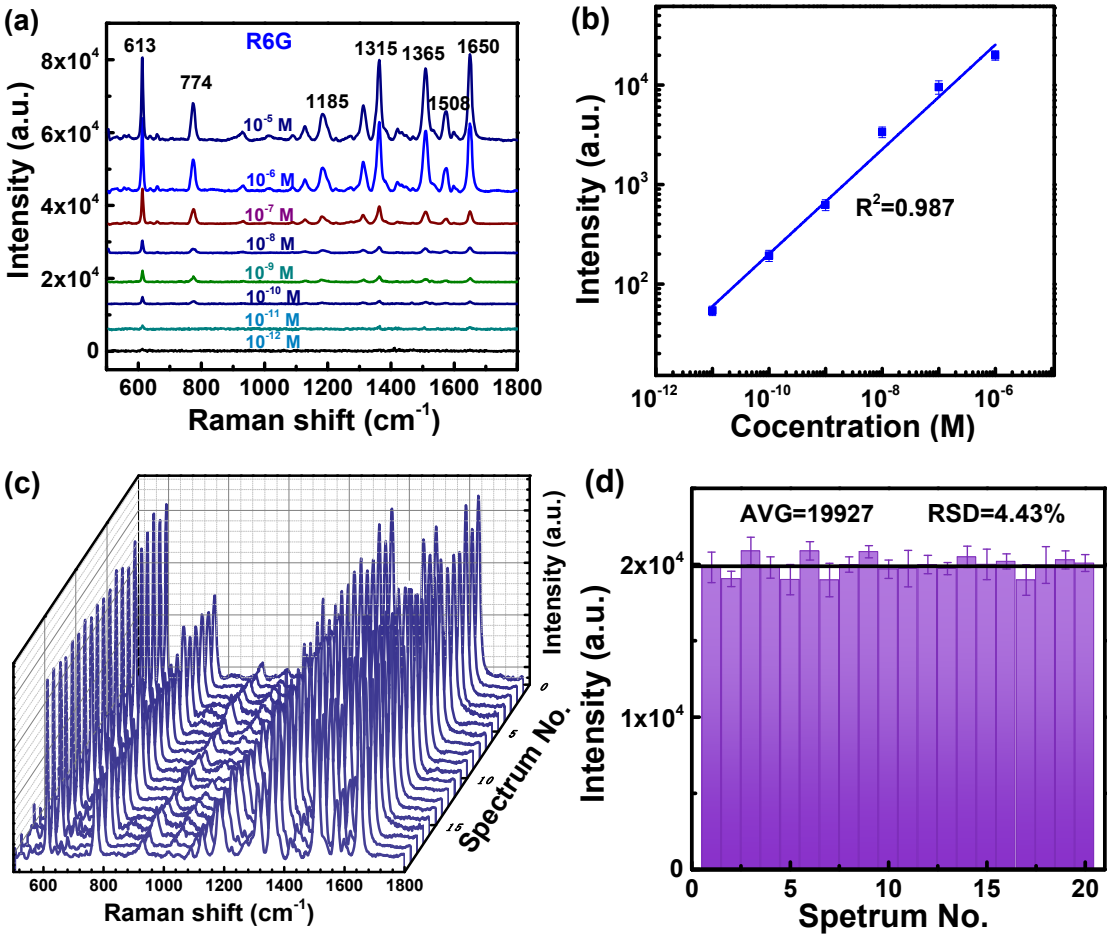

Figure 4: (a) Raman spectra of R6G with different concentrations on the particle-in-multiscale 3D substrate (PDMS)/grating/zinc oxide nano spikes (ZnO NSs)/silver nanoparticles (Ag NPs) substrates. (b) Calibration curve of Raman intensity at 613 cm^{-1} versus the concentration of R6G (10^{-6}~10^{-11} M). (c) Twenty Raman spectra of R6G with a concentration of 10^{-6} M on the substrates from different batches. (d) Intensities distribution of 613 cm^{-1} peaks of the twenty Raman spectra.

spectra of R6G with a concentration of 10^{-6} M have good consistency with each other, and the intensity of the SERS signal is similar for different peaks. The relative intensities at the 613 cm^{-1} peaks for the twenty Raman spectra of R6G are shown in Figure 4d. The error bars in Figure 4d represent the intensity distribution of the 613 cm^{-1} peaks from 10 spots on one sample. The dotted line represents the average intensity of 19,927 from the 20 batches substrates. All relative intensities of the 613 cm^{-1} peak exhibit a minor fluctuation around the average intensity. The RSD of the Raman intensities at 613 cm^{-1} peaks is about 4.43%. These data demonstrate that the homogeneous Raman signal and excellent reproducibility can be realized on the PDMS/grating/ZnO NSs/Ag NPs substrates. To verify the ability to predict concentrations with accuracy in the range of concentrations, the 10 Raman spectra of R6G with a concentration of 3.0×10^{-9} M on the PDMS/grating/ZnO NSs/Ag NPs substrates were randomly collected to estimate the concentration, as shown in Figure S7 [31]. The corresponding Raman intensities of 613 and 774 cm^{-1} are described in Figure S7b and c, respectively. The average Raman intensity of 1211 is obtained from the 10 Raman intensity for 613 cm^{-1}. The calculated concentration of R6G is 3.07×10^{-9} M according to the fitting formula of LogI = 0.54 LogC+7.62 and the average Raman intensity for 613 cm^{-1}. The average Raman intensity of 539 is obtained from the 10 Raman intensity for 774 cm^{-1}. The calculated concentration of R6G is 3.15×10^{-9} M according to the fitting formula of LogI = 0.52LogC+7.15 and the average Raman intensity for 774 cm^{-1}. The error values of 2.3 and 5.0% are obtained between calculated concentration and actual concentration for 613 and 774 cm^{-1}, respectively. The small error values further illustrate the ability of quantitative detection and reproducibility of these SERS substrates.

To investigate the stability of PDMS/grating/ZnO NSs/Ag NPs substrates, two substrates with similar performance are placed in the high-purity nitrogen-filled glovebox or atmospheric environments, respectively. The Raman spectra of R6G molecules with concentrations of 10^{-6} M on these SERS substrates were repeatedly measured after 10 days. The Raman spectra of the two SERS substrates in the high-purity nitrogen-filled glovebox or atmospheric environments with 0 and 10 days are shown in Figure S8. The intensity of the 613 cm^{-1} peak is chosen to compare the instability of the two SERS substrates. The preserved percentages of the intensities for the 613 cm^{-1} peaks are 94 and 58% for the two SERS substrates after 10 days in the high-purity nitrogen-filled glovebox or atmospheric environments, respectively. Therefore, the oxidation of Ag NPs due to aerobic exposure is the main instability factor rather than the complex structure of the substrate. The current commercial packaging technology is very mature, and there is no need to worry about the oxidation of Ag NPs.

To verify the relationship between plasma enhancement and sizes of plasmon NPs, the local electromagnetic field intensity distributions of Ag NPs on the different substrate environments with different diameters (12, 22, and 32 nm) were analyzed by the COMSOL simulations. The simulated structures are PDMS/Ag NPs, PDMS/grating/Ag NPs, and PDMS/grating/ZnO NSs/Ag NPs. The period, the groove width and the groove depth of grating, the gap of Ag NPs, the height of the ZnO NSs, and the waist diameter of the ZnO NSs are 1500, 1000, 170, 2, 462, and 57 nm, respectively. The incident light irradiates perpendicularly onto the surface of the substrate in this simulation. The wavelength of incident light is 532 nm in the simulations of local electromagnetic field intensity distributions, which is consistent with the one used in the Raman characterization experiment. The simulated electromagnetic field intensity distributions and the best 1000 points of simulated electromagnetic field intensities, as shown in Figures S9 and S10. According to the simulation results, the maximum electromagnetic field intensities (E_{max}s) of PDMS/Ag NPs structure are 9.9 times, 15.1 times, and 14.1 times incident electromagnetic field (E_O) for the 12, 22, and 32 nm diameters of Ag NPs. The E_{max}s of PDMS/grating/Ag NPs structure are 10.6 E_O, 18.4 E_O, and 18.5 E_O for the 12, 22, and 32 nm diameters of Ag NPs. The E_{max}s of PDMS/grating/ZnO NSs/Ag NPs structure are 20.5 E_O, 70.5 E_O, and 456.3 E_O for the 12, 22, and 32 nm diameters of Ag NPs. When the gap of Ag NPs remains unchanged, the relationship between the plasma enhancement degree and the sizes of Ag NPs is not a simple linear relationship, which also is dependent on the attached substrate environment of plasmon NPs. The SERS intensities depend not only on the plasma enhancement degree of the plasmon NPs but also on the hot spot area range from Ag NPs. The actual SERS substrate is much more complex than the simulation situation, and the influencing factors are also complex for SERS intensities.

Some contrast substrates with different structures were prepared to investigate the SERS effect and the advantage of PDMS/grating/ZnO NSs/Ag NPs as SERS substrates. The Raman spectra of R6G with concentrations of 10^{-6} or 10^{-3} M for contrast substrates were measured and are shown in Figure 5a. The planar ZnO seed layer has any Raman enhancement to R6G at the concentration of 10^{-3} M, as shown in Figure S11. The weak Raman enhancement of R6G at the concentration of 10^{-3} M is achieved for the PDMS/

ZnO NSs substrates, which may be ascribed to the multiple reflections of incident light in the ZnO NSs structure [32, 33]. The obvious Raman enhancement of R6G at the concentration of 10^{-6} M is achieved for the PDMS/Ag NPs (10 nm deposition thickness of Ag) substrates, which may be ascribed to the surface plasmon resonance of Ag NPs. Compared with the PDMS/Ag NPs substrates, the SERS signal of the PDMS/ZnO NSs/Ag NPs substrates and the PDMS/grating/Ag NPs substrates are both increased, which means that the ZnO NSs structure and the grating structure are both beneficial to enhance the surface plasmon resonance effect of Ag NPs. The SERS intensity of PDMS/grating/ZnO NSs/Ag NPs substrates is the highest, which may benefit from the electromagnetic field enhancement from the excellent optical capture capability of grating/ZnO NSs substrates, and the more and stronger hot spots from Ag NPs in ZnO NSs surface. To illustrate the excellent optical coupling ability of grating/ZnO NSs substrates, the absorption spectra of the different substrates were measured and are shown in Figure 5b. The PDMS/grating substrate has very low absorption in the 300~900 nm, which means that the PDMS has good light transmittance. The absorption spectra of PDMS/ZnO seed substrate have an obvious absorption peak at 334 nm [34, 35]. Compared with the PDMS/ZnO seed substrate, the PDMS/ZnO NSs substrate shows a wider absorption range from 300 to 900 nm and a stronger absorption peak at 334 nm. It means that ZnO NSs have better photon trapping ability due to the multiple reflections of incident light. In the meantime, the ZnO NSs structure is expected to increase the specific surface area of Ag and the nanogaps between adjacent Ag NPs, and thus should be good for getting more and stronger hot spots [36, 37]. The PDMS/Ag NPs substrate shows a wide absorption range from 300 to 900 nm with a strong absorption peak at 475 nm, which is the characteristic LSPR absorption peak of Ag NPs [38]. When the grating structure is added in PDMS of PDMS/Ag NPs or PDMS/ZnO NSs/Ag NPs substrates, the absorption intensities are enhanced in the absorption range from 300 to 900 nm, especially in the position of the corresponding absorption peaks of ZnO NSs and Ag NPs. It indicates that the light capture performance is enhanced by the introduction of the grating, which can improve the Raman scattering efficiency. The diffraction effect of the grating structure may encourage part of the light to generate directional scattering, thereby increasing the effective volume of the medium that interacts with the excitation light [39]. The PDMS/grating/ZnO NSs/Ag NPs substrates have the strongest characteristic LSPR absorption of Ag NPs. The electromagnetic field enhancement may benefit from the excellent optical capture capability of grating/ZnO NSs multiscale 3D structure, the more and stronger hot spots from Ag NPs in ZnO NSs surface. To better understand the enhancement mechanism of this PDMS/grating/ZnO NSs/Ag NPs as SERS substrates, the absorption spectra, and the local electromagnetic field intensity distributions in these structures were analyzed by the COMSOL simulations, as shown in Figure 5c, d. Except that the diameter of Ag NPs is fixed at 22 nm, other simulation parameters remain unchanged. The best 1000 points of simulated electromagnetic field intensities for different substrates are shown in Figure S12. For the planar PDMS/Ag NPs structure, the electromagnetic fields distribute around the Ag NPs owing to the LSPR effect of Ag NPs and hot spots distribute in the lateral nanogaps between the evaporated Ag NPs on the surface [40]. The E_{max} of PDMS/Ag NPs structure is 15.1 times E_0. The E_{max} of PDMS/grating/Ag NPs structure is 18.4 times E_0, which is higher than that of the planar PDMS/Ag NPs structure. This coupling effect between the LSPR of Ag NPs and the diffraction effect of the grating structure can be understood to strengthen the LSPR. The E_{max} of 3.5 times E_0 for PDMS/ZnO NSs structures means that the electromagnetic field can be slightly enhanced inside the ZnO NSs structures, which may be mainly caused by the efficient scattering light coupling. Compared with PDMS decorated with Ag NPs, PDMS/ZnO NSs/Ag NPs structure exhibits much stronger electromagnetic field enhancement effects. This coupling effect of the LSPR of Ag NPs and the photon trapping ability of the ZnO NSs structure can be also understood to strengthen the LSPR. In the meantime, the high-density and homogeneous spatial hot spots are formed in the PDMS/ZnO NSs/Ag NPs structure due to the increased specific surface area of Ag and nanogaps between adjacent Ag NPs. The ZnO NSs on PDMS can load more and closer Ag NPs to form dense hot spots, resulting in a larger electromagnetic field than that of the PDMS, which is consistent with Raman results of these two substrates [41]. The E_{max} of PDMS/ZnO NSs/Ag NPs structure is increased 66.3 times E_0, which is found between Ag NPs that adhere to the intersection of two ZnO NSs. The electromagnetic field enhancement around Ag NP for PDMS/grating/ZnO NSs/Ag NPs structure is higher compared with PDMS/grating/Ag NPs or PDMS/ZnO NSs/Ag NPs structures. The E_{max} of PDMS/grating/ZnO NSs/Ag NPs structure is increased 70.5 times E_0. It means that the LSPR of Ag NPs can be significantly enhanced by the cascaded optical field enhancement of the grating and the ZnO NSs structure. The variation trend of the simulated absorption spectrum intensity for different substrates is similar to

that of the simulated electromagnetic field intensities and measured absorption spectra, especially at 532 nm.

To further investigate the SERS performance of the PDMS/grating/ZnO NSs/Ag NPs substrates, the Raman spectra of CV molecules with different concentrations from 10^{-6} to 10^{-11} M on the 3D substrates are shown in Figure 6a. All the Raman spectra were collected under the same conditions. The Raman characteristic peaks (922, 1182, 1375, 1536, 1590, and 1622 cm^{-1}) of CV can be observed in all the Raman spectra for CV with different concentrations. The typical Raman spectrum can still be observed even at a low concentration of 10^{-11} M for CV, which further indicates that the PDMS/grating/ZnO NSs/Ag NPs as SERS substrates have a high sensitivity. The Raman intensities are weakened with the decrease of the CV concentrations. The linear fit calibration curve ($R^2 = 0.988$) with error bars is illustrated in Figure 6b. The logarithm intensities of the SERS spectra of CV are proportional to the logarithm of the concentrations of the CV. Therefore, the proposed substrate shows great potential for identifying trace molecules due to dense hot spots.

To investigate the potential of the PDMS/grating/ZnO NSs/Ag NPs substrates in practical application, the SERS detection for malachite green (MG) molecule was carried out and are shown in Figure 7a. The MG molecule is a chemical of poisonous triphenylmethane, which is a harmful carcinogen, will render malformation and mutagenic side effects. Many countries have taken actions to prohibit the abuse of MG in marine products. However, the MG molecule is still frequently and illegally used as fungicide, antiseptic ectoparasiticide in aquaculture to improve the survival rate of aquatic products. Consequently, the effective detection of

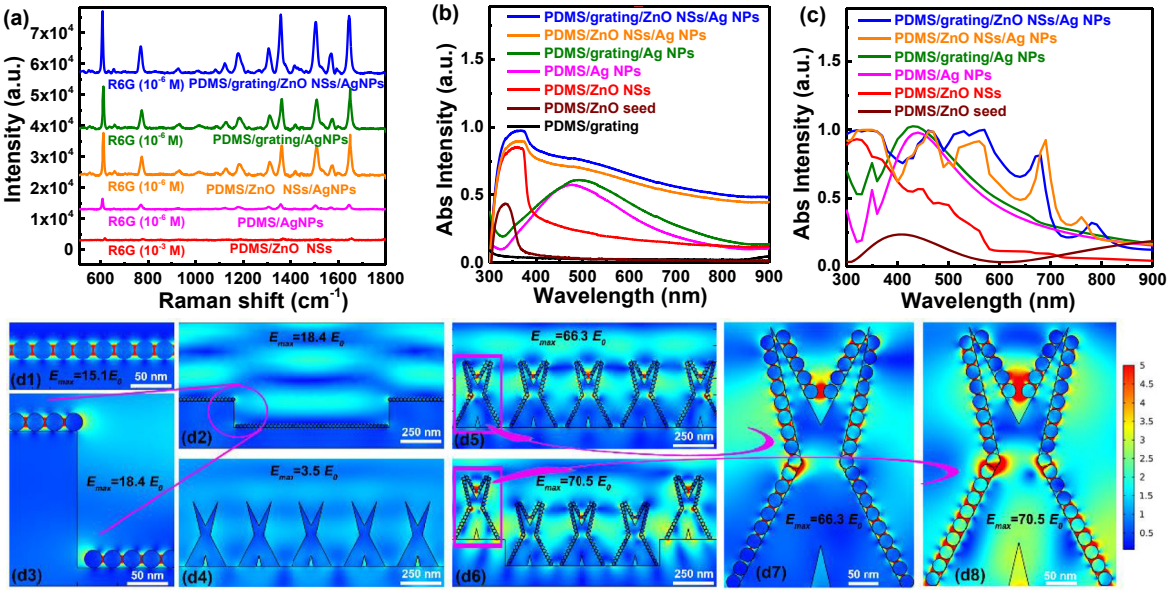

Figure 5: (a) Raman spectra of R6G on different substrates. Measured absorption spectra (b) and simulated absorption spectra (c) of different substrates. (d) Simulated electromagnetic field intensity distributions at 532 nm of the particle-in-multiscale 3D substrate (PDMS)/silver nanoparticles (Ag NPs) (d1), PDMS/grating/Ag NPs (d2 and d3), PDMS/zinc oxide nano spikes (ZnO NSs) (d4) PDMS/ZnO NSs/Ag NPs (d5 and d7) and PDMS/ZnO NSs/Ag NPs (d6 and d8) substrates.

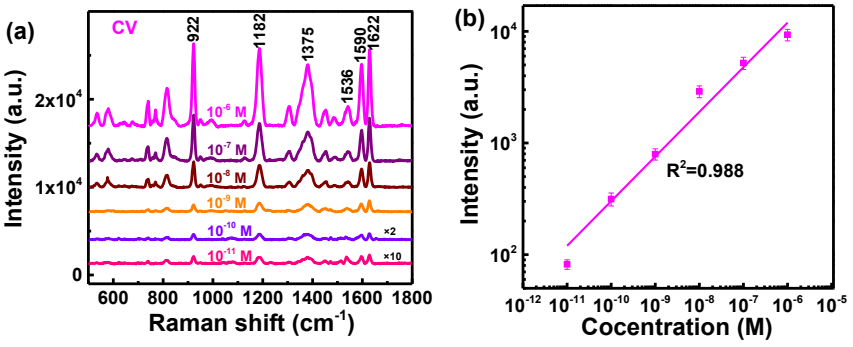

Figure 6: (a) Raman spectra of CV on the particle-in-multiscale 3D substrate (PDMS)/grating/zinc oxide nano spikes (ZnO NSs)/silver nanoparticles (Ag NPs) substrates. (b) Calibration curve of Raman intensity at 922 cm^{-1} versus the concentration of CV.

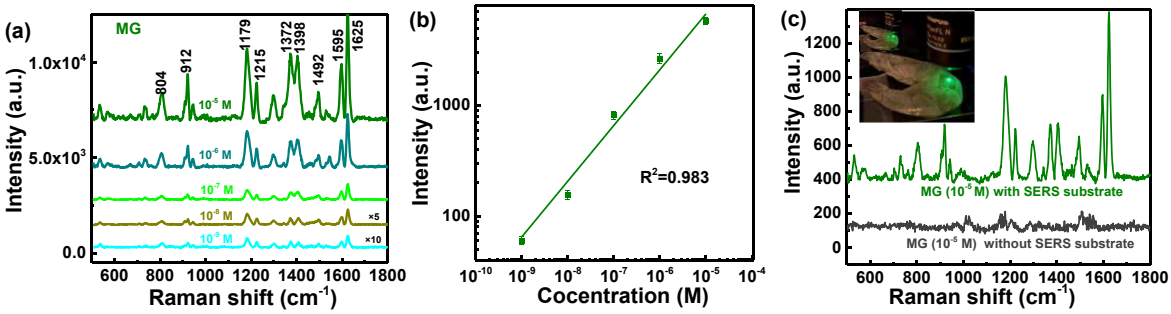

Figure 7: (a) Raman spectra of MG on the particle-in-multiscale 3D substrate (PDMS)/grating/zinc oxide nano spikes (ZnO NSs)/silver nanoparticles (Ag NPs) substrates. (b) Calibration curve of Raman intensity at 1625 cm^{-1} versus the concentration of MG. (c) Raman spectra of MG on the surface of shrimp.

the MG molecule in aquatic products is very necessary for human health. The typical Raman peaks of the MG molecule at 912, 1179, 1372, and 1625 cm^{-1} have a sharp form at a high concentration of 10^{-5} M. The Raman intensities are weakened with the decrease of the MG molecule concentrations. The main characteristic peaks such as 1179, 1372, and 1625 cm^{-1} could be observed at a concentration lower down to 10^{-9} M. The linear fit calibration curve (R^2 = 0.982) with error bars is illustrated in Figure 7b. The logarithm intensities of the SERS spectra of the MG molecule are proportional to the logarithm of the concentrations of the MG molecule, which indicates the promising application prospects of this substrate. For practical application, the *in-situ* detections of vestigial MG molecule on shrimp surface were executed using the semi-transparent flexible PDMS/grating/ZnO NSs/Ag NPs substrate and without SERS substrate. The shrimp surface was immersed in 10^{-5} M MG solution for 12 h. The Raman signals of the MG molecule on the shrimp surface are shown in Figure 7c. The characteristic peaks of MG including 912, 1179, 1372, and 1625 cm^{-1} can be found in shrimp surface, when the semi-transparent flexible PDMS/grating/ZnO NSs/Ag NPs as SERS substrate was stuck onto the shrimp surface. In the contrast, the Raman signal of the MG molecule is not observed in the shrimp surface without SERS substrate. In this experiment, it is indispensable to use a flexible substrate with grating/ZnO NSs/Ag NPs structure to contact the surface of shrimp. Due to the excellent transparency of PDMS, the laser can penetrate the PDMS layer to access the Ag NPs layer. Aquatic products contaminated with MG residues above the concentration level (1 ng/g in the USA and 2 ng/g in the EU) have been tested for carcinogenicity [42]. The probe molecules MG were dissolved in ethanol to obtain the MG solution of 10^{-5} M concentration. The concentration of 10^{-5} M for MG solution is equal to 58.6 ng/g according to the density of 0.79 g/ml for ethanol and the relative molecular mass of 463.5. The concentration of 10^{-5} M for MG solution is much lower than the concentration level required by the EU and USA, which is completely satisfied for the use of the practical detection. A series of test results strongly demonstrate the practical significance of the semi-transparent flexible PDMS/grating/ZnO NSs/Ag NPs substrate in the rapid detection of surface analyses.

3 Conclusions

In summary, the particle-in-multiscale 3D substrate of PDMS/grating/ZnO NSs/Ag NPs is successfully applied in the SERS area due to the excellent optical capture capability of grating/ZnO NSs multiscale structure and abundant electromagnetic hot spots. The optimized particle-in-multiscale 3D substrate presents high sensitivity with an ultralow LOD of 1×10^{-11} M and a high EF of 7.0×10^8, the quantitative analysis ability, excellent homogeneity, and reproducibility for R6G as the probe molecule. This substrate also exhibits superior detection capacity for CV and MG. In addition, these SERS substrates can realize *in-situ* detection of MG Raman signal in shrimp surface due to its excellent light transmission and flexibility. A series of test results demonstrate the particle-in-multiscale 3D structure as SERS substrates exhibit the vast potential in practical applicability for qualitatively and quantitatively chemical and biomedical analysis.

Author contributions: All the authors have accepted responsibility for the entire content of this submitted manuscript and approved submission.

Research funding: The authors acknowledge the financial support from the National Natural Science Foundation of China (12047537, 1210040375, 12074229, 62075155), Chinese Postdoctoral Science Foundation (2017M622251), Shandong Provincial Natural Science Foundation (ZR2017BF027, ZR2018MA040), State Key Laboratory of Bio-polysaccharide Fiber Forming and Eco-Textile (KF2020204), and Key R&D

and Promotion (Science and Technology Research) Project of Henan Province (192102310027).

Conflict of interest statement: The authors declare no conflicts of interest regarding this article.

References

[1] W. Kim, J. Park, W. Kim, S. Jo, and J. Park, "Bio-inspired Ag nanovilli-based sandwich-type SERS aptasensor for ultrasensitive and selective detection of 25-hydroxy vitamin D3," *Biosens. Bioelectron.*, vol. 188, p. 113341, 2021.

[2] C. Li, S. Xu, J. Yu, Z. Li, and C. Zhang, "Local hot charge density regulation: vibration-free pyroelectric nanogenerator for effectively enhancing catalysis and in-situ surface enhanced Raman scattering monitoring," *Nano Energy*, vol. 81, p. 105585, 2021.

[3] G. Wang, H. Wei, Y. Tian, et al., "Twin-ZnSe nanowires as surface enhanced Raman scattering substrate with significant enhancement factor upon defect," *Opt. Express*, vol. 28, no. 13, pp. 18843–18858, 2020.

[4] C. Zhang, S. Chen, Z. Jiang, Z. Shi, J. Wang, and L. Du, "Highly sensitive and reproducible SERS substrates based on ordered micropyramid array and silver nanoparticles," *ACS Appl. Mater. Interfaces*, vol. 13, no. 24, pp. 29222–29229, 2021.

[5] Z. Zuo, L. Sun, Y. Guo, et al., "Multiple plasmon couplings in 3D hybrid Au-nanoparticles-decorated Ag nanocone arrays boosting highly sensitive surface enhanced Raman scattering," *Nano Res.*, p. 9, 2021, https://doi.org/10.1007/s12274-021-3477-x.

[6] X. Xiu, L. Hou, J. Yu, S. Jiang, and Z. Li, "Manipulating the surface-enhanced Raman spectroscopy (SERS) activity and plasmon-driven catalytic efficiency by the control of Ag NP/graphene layers under optical excitation," *Nanophotonics*, vol. 10, no. 5, pp. 1529–1540, 2021.

[7] C. Li, S. Xu, J. Yu, et al., "3D hybrid MoS_2/AgNPs/inverted pyramid PMMA resonant cavity system for the excellent flexible surface enhanced Raman scattering sensor," *Sensor. Actuator. B Chem.*, vol. 274, no. 20, pp. 152–162, 2018.

[8] N. Mueller, E. Pfitzner, Y. Okamura, et al., "Surface-enhanced Raman scattering and surface-enhanced infrared absorption by plasmon polaritons in three-dimensional nanoparticle supercrystals," *ACS Nano*, vol. 15, no. 3, pp. 5523–5533, 2021.

[9] H. Guan, W. Li, J. Han, et al., "General molten-salt route to three-dimensional porous transition metal nitrides as sensitive and stable Raman substrates," *Nat. Commun.*, vol. 12, no. 1, p. 11, 2021.

[10] X. Hu, B. Yang, X. Wen, et al., "One-pot synthesis of a three-dimensional Au-decorated cellulose nanocomposite as a surface-enhanced Raman scattering sensor for selective detection and in situ monitoring," *ACS Sustain. Chem. Eng.*, vol. 9, no. 8, pp. 3324–3336, 2021.

[11] Y. Wen, L. Zhen, Z. Lu, Y. Jing, and Z. Chao, "Graphene-Ag nanoparticles-cicada wings hybrid system for obvious SERS performance and DNA molecular detection," *Opt. Express*, vol. 27, no. 3, pp. 3000–3013, 2019.

[12] P. Kumar, R. Khosla, M. Soni, D. Deva, and S. K. Sharma, "A highly sensitive, flexible SERS sensor for malachite green detection based on Ag decorated microstructured PDMS substrate fabricated from Taro leaf as template," *Sensor. Actuator. B Chem.*, vol. 246, pp. 477–486, 2017.

[13] S. Chou, C. Yu, Y. Yen, K. Lin, and H. Chen, "Romantic story or Raman scattering rose petals as ecofriendly, low-cost substrates for ultrasensitive surface-enhanced Raman scattering," *Anal. Chem.*, vol. 87, no. 12, pp. 6017–6024, 2015.

[14] S. Wu, Y. Shen, and C. Jin, "Surface-enhanced Raman scattering induced by the coupling of the guided mode with localized surface plasmon resonances," *Nanoscale*, vol. 11, no. 30, pp. 14164–14173, 2019.

[15] J. Dong, Y. Cao, Q. Han, W. Gao, and J. Qi, "Nanoscale flexible Ag grating/AuNPs self-assembly hybrid for ultra-sensitive sensor," *Nanotechnology*, vol. 32, no. 15, p. 156603, 2020.

[16] N. Chamuah, A. Saikia, A. Joseph, and P. Nath, "Blu-ray DVD as SERS substrate for reliable detection of albumin, creatinine and urea in urine," *Sensor. Actuator. B Chem.*, vol. 285, pp. 108–115, 2019.

[17] C. Han, Y. Wei, F. Lei, et al, "Heterostructured CuO@ZnO@Ag biomimetic setaria as wettability-switchable difunctional SERS substrate for trace pesticide and DNA detections," *Nanophotonics*, vol. 10, 2021. https://doi.org/10.1515/nanoph-2021-0179.

[18] X. Jin, Q. Zhu, L. Feng, X. Li, and G. Shi, "Light-trapping SERS substrate with regular bioinspired arrays for detecting trace dyes," *ACS Appl. Mater. Interfaces*, vol. 13, no. 9, pp. 11535–11542, 2021.

[19] X. Zhao, C. Liu, J. Yu, et al., "Hydrophobic multiscale cavities for high-performance and self-cleaning surface-enhanced Raman spectroscopy (SERS) sensing," *Nanophotonics*, vol. 9, no. 16, pp. 4761–4773, 2020.

[20] J. Xu, Y. Si, Z. Li, S. Jiang, and C. Zhang, "Multiscale structure enabled effective plasmon coupling and molecular enriching for SERS detection," *Appl. Surf. Sci.*, vol. 544, p. 148908, 2021.

[21] H. Wang, J. Yu, H. Liu, and X. Xu, "Low temperature, rapid and controllable growth of highly crystalline ZnO nanostructures via a diluent hydrolytic process and its application to transparent super-wetting films," *CrystEngComm*, vol. 20, no. 3, p. 773, 2018.

[22] A. Pal, S. Pagal, K. Prashanth, G. Chandra, and D. Mohan, "Ag/ZnO/Au 3D hybrid structured reusable SERS substrate as highly sensitive platform for DNA detection," *Sensor. Actuator. B Chem.*, vol. 279, pp. 157–169, 2018.

[23] J. Yu, M. Yang, Z. Li, C. Liu, and F. Lei, "Hierarchical particle-in-quasicavity architecture for ultratrace in situ Raman sensing and its application in real-time monitoring of toxic pollutants," *Anal. Chem.*, vol. 92, no. 21, pp. 14754–14761, 2020.

[24] M. Shafi, R. Liu, Z. Zha, et al., "Highly efficient SERS substrates with different Ag interparticle nanogaps based on hyperbolic metamaterials," *Appl. Surf. Sci.*, vol. 555, p. 149729, 2021.

[25] N. Barveen, T. Wang, Y. Chang, and Z. Liu, "Ultrasensitive and reusable SERS probe for the detection of synthetic dyes in food industry through hybrid flower-shaped ZnO@Ag nanostructures," *J. Alloys Compd.*, vol. 861, p. 157952, 2021.

[26] X. He, Y. Liu, Y. Liu, S. Cui, W. Liu, and Z. Li, "Controllable fabrication of Ag-NP-decorated porous ZnO nanosheet arrays with superhydrophobic properties for high performance SERS detection of explosives," *CrystEngComm*, vol. 22, no. 4, pp. 776–785, 2020.

[27] L. Yang, Y. Yang, Y. Ma, et al., "Fabrication of semiconductor ZnO nanostructures for versatile SERS application," *Nanomaterials*, vol. 7, no. 11, p. 398, 2017.

[28] A. Bolz, U. Panne, K. Rurack, and M. Buurman, "Glass fibre paper-based test strips for sensitive SERS sensing," *Anal. Methods*, vol. 8, no. 6, pp. 1313–1318, 2016.
[29] D. Xu, M. Muhammad, L. Chu, Q. Sun, C. Shen, and Q. Huang, "SERS approach to probe the adsorption process of trace volatile benzaldehyde on layered double hydroxide material," *Anal. Chem.*, vol. 93, no. 23, pp. 8228–8237, 2021.
[30] C. Haynes, C. Yonzon, X. Zhang, and R. Duyne, "Surface-enhanced Raman sensors: early history and the development of sensors for quantitative biowarfare agent and glucose detection," *J. Raman Spectrosc.*, vol. 36, nos 6–7, pp. 471–484, 2005.
[31] S. Bell, G. Charron, E. Cortés, et al., "Towards reliable and quantitative surface-enhanced Raman scattering (SERS): from key parameters to good analytical practice," *Angew. Chem. Int. Ed.*, vol. 59, no. 14, pp. 5454–5462, 2020.
[32] J. Yu, Y. Guo, H. Wang, S. Su, and F. Lei, "Quasi optical cavity of hierarchical ZnO nanosheets@Ag nanoravines with synergy of near- and far-field effects for in situ Raman detection," *J. Phys. Chem. Lett.*, vol. 10, no. 13, pp. 3676–3680, 2019.
[33] H. Shin, E. Shim, Y. Choi, J. Park, and S. Yoon, "Giant enhancement of the Raman response due to one-dimensional ZnO nanostructures," *Nanoscale*, vol. 6, no. 24, pp. 14622–14626, 2014.
[34] M. Liu, Y. Xu, Z. Gao, C. Zhang, and Q. Sun, "Natural biomaterial sarcosine as an interfacial layer enables inverted organic solar cells exhibiting over 16.4% efficiency," *Nanoscale*, vol. 13, pp. 11128–11137, 2021.
[35] Y. Wang, F. Wang, J. Gao, et al., "Organic photovoltaics with 300 nm thick ternary active layer exhibiting 15.6% efficiency," *J. Mater. Chem. C*, vol. 9, pp. 9892–9898, 2021.
[36] D. Tieu, T. Trang, V. Le, and V. Thu, "Assembly engineering of Ag@ZnO hierarchical nanorod arrays as a pathway for highly reproducible surface-enhanced Raman spectroscopy applications," *J. Alloys Compd.*, vol. 808, p. 151735, 2019.
[37] T. Fang, M. Zhang, Z. Li, et al., "Hexagonally arranged arrays of urchin-like Ag-nanoparticle decorated ZnO-nanorods grafted on PAN-nanopillars as surface-enhanced Raman scattering substrates," *CrystEngComm*, vol. 20, no. 25, pp. 3550–3558, 2018.
[38] Q. Sun, Q. Zhang, N. Zhou, et al., "Silver-coated flower-like ZnO nanorod arrays: ultrastable SERS substrates and the mechanisms of optical stability," *Appl. Surf. Sci.*, vol. 526, p. 146565, 2020.
[39] J. Wang, Z. Jia, and C. Lv, "Enhanced Raman scattering in porous silicon grating," *Opt. Express*, vol. 26, no. 6, pp. 6507–6518, 2018.
[40] X. Zhao, C. Li, Z. Li, J. Yu, and B. Man, "In-situ electrospun aligned and maize-like AgNPs/PVA@Ag nanofibers for surface-enhanced Raman scattering on arbitrary surface," *Nanophotonics*, vol. 8, no. 10, pp. 1719–1729, 2019.
[41] S. Li, N. Zhang, N. Zhang, D. Lin, X. Yang, "Three-dimensional ordered Ag/ZnO/Si hierarchical nanoflower arrays for spatially uniform and ultrasensitive SERS detection," *Sensor. Actuator. B Chem.*, vol. 321, p. 128519, 2020.
[42] Z. Li, S. Jiang, Y. Huo, et al., "3D silver nanoparticles with multilayer graphene oxide as a spacer for surface enhanced Raman spectroscopy analysis," *Nanoscale*, vol. 10, no. 13, pp. 5897–5905, 2018.

Supplementary Material: The online version of this article offers supplementary material (https://doi.org/10.1515/nanoph-2021-0381).